

Angular power spectrum of galaxies in the 2MASS Redshift Survey

Shin'ichiro Ando,^{1,2} Aurélien Benoit-Lévy,³ and Eiichiro Komatsu^{4,2}

¹*GRAPPA Institute, University of Amsterdam, 1098XH Amsterdam, Netherlands*

²*Kavli Institute for the Physics and Mathematics of the Universe (Kavli IPMU, WPI), Todai Institutes for Advanced Study, University of Tokyo, Kashiwa 277-8583, Japan*

³*Sorbonne Universités, UPMC Univ Paris 6 et CNRS, UMR 7095, Institut d'Astrophysique de Paris, 75014 Paris, France*

⁴*Max-Planck-Institut für Astrophysik, Karl-Schwarzschild Strasse 1, 85748 Garching, Germany*

16 June 2017; accepted 6 October 2017

ABSTRACT

We present the measurement and interpretation of the angular power spectrum of nearby galaxies in the 2MASS Redshift Survey catalog with spectroscopic redshifts up to $z \approx 0.1$. We detect the angular power spectrum up to a multipole of $\ell \approx 1000$. We find that the measured power spectrum is dominated by galaxies living inside nearby galaxy clusters and groups. We use the halo occupation distribution (HOD) formalism to model the power spectrum, obtaining a fit with reasonable parameters. These HOD parameters are in agreement with the 2MASS galaxy distribution we measure toward the known nearby galaxy clusters, confirming validity of our analysis.

Key words: galaxies: fundamental parameters — large-scale structure of Universe

1 INTRODUCTION

The 2MASS Redshift Survey (2MRS; Huchra et al. 2012) is a spectroscopic follow-up of galaxies detected in the photometric Two Micron All Sky Survey (2MASS; Skrutskie et al. 2006). The 2MRS provides an excellent probe of the *nearby* distribution of galaxies up to $z \approx 0.1$. Among many applications of this full-sky map of galaxies, one powerful application is the cross-correlation with a map of different tracers with unknown redshifts.

For example, the cross correlation of the photometric 2MASS galaxies with the cosmic microwave background (CMB) temperature map was used to measure a dynamical signature of dark energy in the CMB via the integrated Sachs-Wolfe effect (Afshordi et al. 2004). The cross-correlation with a gamma-ray map measured by Large Area Telescope (LAT) of the Fermi satellite has an excellent sensitivity to gamma-rays from annihilation of dark matter particles (Xia et al. 2011; Ando et al. 2014; Cuoco et al. 2015). The cross correlation of the 2MRS catalog with a map of the thermal Sunyaev-Zeldovich effect derived from the Planck data (Planck Collaboration 2016a) has been measured recently (Makiya et al. 2017), and it tells us how hot gas traces galaxies in the nearby Universe.

To understand properly various such measurements of cross correlations, we must understand clustering of galaxies in the 2MRS catalog, i.e., the auto power spectrum of 2MRS. In this paper, we present the measurement and interpretation of the 2MRS angular power spectrum. Frith

et al. (2005) presented the angular power spectrum of the 2MASS full release extended source catalog.

Throughout the paper, we adopt cosmological parameters of Planck Collaboration (2016b, Table 4, TT+lowP+lensing). We define a halo mass ($M \equiv M_{\text{vir}}$) as a mass enclosed within a virial radius r_{vir} , within which the average matter density is $\Delta_{\text{vir}}(z)$ times the critical density $\rho_c(z)$, where $\Delta_{\text{vir}}(z) \equiv 18\pi^2 + 82d - 39d^2$ with $d \equiv \Omega_m(1+z)^3/[\Omega_m(1+z)^3 + \Omega_\Lambda] - 1$ (Bryan & Norman 1998). Conversion from other definitions of the mass (such as M_{200} defined with radius r_{200} within which the average density is 200 times the critical density) is done by assuming a Navarro-Frenk-White density profile (Navarro et al. 1997) and using fitting formulae given in Hu & Kravtsov (2003).

2 ANGULAR POWER SPECTRUM

2.1 Construction of the galaxy density map

We construct a pixelized count map of the 2MRS galaxies using the HEALPix¹ scheme on the sphere, with the resolution parameter of $N_{\text{side}} = 512$. We then construct a map of the galaxy density contrast as

$$\delta_g = \frac{n_g - \bar{n}_g}{\bar{n}_g}, \quad (1)$$

¹ <http://healpix.sourceforge.net>

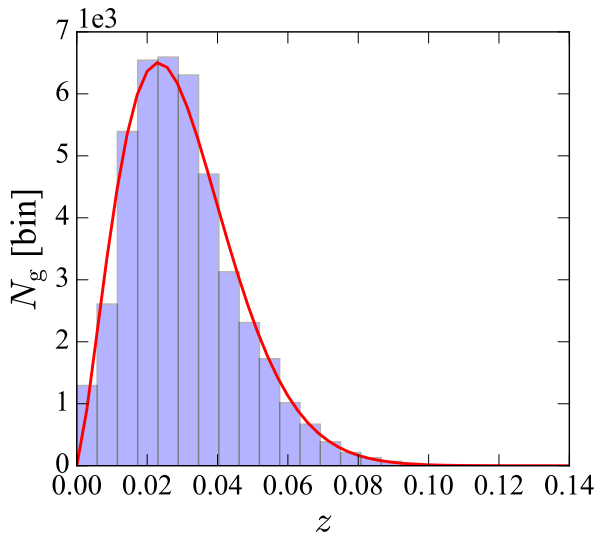


Figure 1. The number of 2MRS galaxies in each redshift bin, compared with the fitting function, equation. (2).

where \bar{n}_g is the mean number of galaxies per pixel, and n_g is the number of galaxies in a given pixel.

We avoid regions close to the Galactic plane by masking pixels in $|b| < 5^\circ$ for $30^\circ < l < 330^\circ$ and $|b| < 10^\circ$ otherwise. In addition we mask small regions that have very low redshift completeness as computed by Lavaux & Hudson (2011) (the white regions in the left panel of their figure 4). The fraction of sky available for the analysis is $f_{\text{sky}} = 0.877$.

The redshift distribution of the 2MRS galaxies is well approximated by

$$\frac{dN_g}{dz} = \frac{N_g \beta}{z_0 \Gamma[(m+1)/\beta]} \left(\frac{z}{z_0}\right)^m \exp\left[-\left(\frac{z}{z_0}\right)^\beta\right], \quad (2)$$

where $N_g = 43182$ is the total number of the galaxies in the 2MRS catalog in the unmasked pixels. We performed an unbinned likelihood analysis and found $m = 1.31$, $\beta = 1.64$, and $z_0 = 0.0266$. Figure 1 shows dN_g/dz of the 2MRS galaxies.

Redshifts of the 2MRS are claimed to be complete for galaxies up to a magnitude of $K_s = 11.75$, and are nearly volume-limited up to $z \approx 0.02$. Completeness of redshifts as computed by Lavaux & Hudson (2011) is quite homogeneous except small regions that have very low completeness. We mask those regions as described above, and apply no completeness correction for the derived δ_g .

2.2 Estimation of the angular power spectrum

We used the publicly available software PolSpice² to estimate the angular power spectrum of δ_g . PolSpice allows for an efficient de-convolution of the harmonic couplings induced by the mask.

The estimated angular power spectrum, C_ℓ , is the sum of the signal and the shot noise, and the latter needs to be subtracted. The shot noise is usually assumed to be equal to

$1/\bar{n}_g$, but this simple relation may not always hold due to halo exclusion and non-linear effects (Baldauf et al. 2013). We thus employ here another route to disentangle signal and noise. We consider a half-sum (HS) and a half-difference (HD) of the data to obtain directly a noise estimate. Instead of generating a single density map from a given catalog, we first divide the catalog into two subsets by randomly selecting half the galaxies, and construct two galaxy density maps $\delta_{g,1}$ and $\delta_{g,2}$. We then form the following maps:

$$HS = \frac{\delta_{g,1} + \delta_{g,2}}{2}, \quad HD = \frac{\delta_{g,1} - \delta_{g,2}}{2}, \quad (3)$$

As the division of the catalog into subsets is a random process, the estimated HD changes slightly depending on realizations. These changes do not affect our conclusion, but we shall explore the impacts of randomness on the best-fitting model parameters in Sec. 4.1.

The power spectrum extracted from the HS map contains both the signal and noise, whereas that from the HD map contains only the noise. Hence our estimator for the angular power spectrum is given by

$$\hat{C}_\ell = C_\ell^{HS} - C_\ell^{HD}. \quad (4)$$

We present the measured power spectrum minus the noise power in figure 2. We detect the power spectrum clearly all the way to the maximum multipole reliably resolved by the HEALPix map with $N_{\text{side}} = 512$, i.e., $\ell_{\text{max}} = 2N_{\text{side}} = 1024$. This indicates that the 2MRS galaxies are strongly clustered: we have 43182 galaxies over 87.7% of the sky, and thus the mean galaxy number density is only 1.2 deg^{-2} . As we show in this paper, many of the 2MRS galaxies reside in galaxy clusters and groups, producing power at multipoles much higher than that of the mean separation of galaxies.

We tabulate the measured power spectrum data with diagonal elements of the covariance matrix in Table 1.

2.3 Covariance matrix

To estimate the covariance matrix of the power spectrum, $\text{Cov}(C_\ell, C_{\ell'}) \equiv \langle (C_\ell - \langle C_\ell \rangle)(C_{\ell'} - \langle C_{\ell'} \rangle) \rangle$ where $\langle \dots \rangle$ denotes the ensemble average, we take a two-step approach. We first start with a diagonal Gaussian covariance given by

$$\text{Cov}(C_\ell, C_{\ell'})_{\text{Gauss}} = \frac{2(C_\ell^{\text{tot}})^2 \delta_{\ell\ell'}}{f_{\text{sky}}(2\ell+1)\Delta\ell}, \quad (5)$$

where $\delta_{\ell\ell'}$ is the Kronecker delta, $\Delta\ell$ is the size of multipole bins, f_{sky} is the sky fraction used in the analysis, and C_ℓ^{tot} is the sum of the signal and the noise power, i.e., $C_\ell^{\text{tot}} = C_\ell^{HS}$. To reduce an artificial scatter in the covariance matrix, we smooth the measured total power spectrum before computing the covariance matrix.

To this Gaussian covariance, we add a non-Gaussian contribution from the connected part of the trispectrum, $T_{\ell\ell'}$, as (e.g., Komatsu & Seljak 2002)

$$\text{Cov}(C_\ell, C_{\ell'}) = \frac{1}{f_{\text{sky}}} \left[\frac{2(C_\ell^{\text{tot}})^2 \delta_{\ell\ell'}}{(2\ell+1)\Delta\ell} + \frac{T_{\ell\ell'}}{4\pi} \right]. \quad (6)$$

While the trispectrum term is usually ignored in the galaxy power spectrum analysis, it is important for the 2MRS angular power spectrum because the power spectrum is dominated by galaxies living inside nearby clusters and groups.

² <http://www2.iap.fr/users/hivon/software/PolSpice/>

Table 1. Power spectrum of the 2MRS, the Gaussian variance, and the total variance.

Mean multipole	Multipole range	ℓC_ℓ [10^{-2} sr]	$\sqrt{\text{Cov}(\ell C_\ell, \ell C_\ell)_{\text{Gauss}}}$ [10^{-2} sr]	$\sqrt{\text{Cov}(\ell C_\ell, \ell C_\ell)}$ [10^{-2} sr]
27	$2 \leq \ell < 53$	6.11	0.32	0.50
78	$53 \leq \ell < 104$	4.88	0.12	0.36
129	$104 \leq \ell < 155$	4.40	0.10	0.29
180	$155 \leq \ell < 206$	4.33	0.10	0.24
231	$206 \leq \ell < 257$	4.03	0.10	0.20
282	$257 \leq \ell < 308$	3.67	0.10	0.18
333	$308 \leq \ell < 359$	3.46	0.10	0.16
384	$359 \leq \ell < 410$	3.47	0.11	0.15
435	$410 \leq \ell < 461$	3.45	0.11	0.15
487	$461 \leq \ell < 513$	3.22	0.11	0.14
538	$513 \leq \ell < 564$	3.14	0.12	0.14
589	$564 \leq \ell < 615$	3.33	0.12	0.14
640	$615 \leq \ell < 666$	2.68	0.13	0.14
691	$666 \leq \ell < 717$	3.00	0.14	0.15
742	$717 \leq \ell < 768$	2.82	0.14	0.15
793	$768 \leq \ell < 819$	2.90	0.15	0.16
844	$819 \leq \ell < 870$	2.90	0.16	0.16
895	$870 \leq \ell < 921$	3.19	0.17	0.17
946	$921 \leq \ell < 972$	2.79	0.18	0.18
998	$972 \leq \ell < 1024$	2.68	0.18	0.19

One may understand this intuitively by noting that the presence of a few nearby massive clusters adds power at all multipoles (see Sec. 4.2) and thus different multipole bins become strongly correlated. This is the sign that the trispectrum term is important.

We shall describe details of the computation of $T_{\ell\ell'}$ in Sec. 4.1, and only outline our procedure here. As the trispectrum term depends on the model of the power spectrum itself, we cannot calculate $T_{\ell\ell'}$ *a priori*. Thus, we first determine the model parameters using the Gaussian covariance in the likelihood analysis. We then calculate $T_{\ell\ell'}$ for the best-fitting model parameters, and re-determine the model parameters using the sum of the Gaussian term and $T_{\ell\ell'}$ in the likelihood. The error bars shown in figure 2 are the diagonal elements of the total covariance matrix including the trispectrum term.

The square-root of the diagonal elements of the Gaussian and total covariance matrices are reported in Table 1.

3 MODEL

3.1 Halo model

We use a halo model (Seljak 2000) to compute the model galaxy power spectrum. We assume that galaxies reside in virialized dark matter halos. In this framework, the galaxy power spectrum is divided into one-halo (1h) and two-halo (2h) terms as $P_g(k, z) = P_g^{1h}(k, z) + P_g^{2h}(k, z)$, where

$$P_g^{1h}(k, z) = \frac{1}{\langle n_g(z) \rangle^2} \int dM \frac{dn}{dM} [2\langle N_{\text{sat}}|M \rangle \tilde{u}_{\text{sat}}(k, M) + \langle N_{\text{sat}}|M \rangle^2 |\tilde{u}_{\text{sat}}(k, M)|^2], \quad (7)$$

$$P_g^{2h}(k, z) = b_g^2(k, z) P_{\text{lin}}(k, z). \quad (8)$$

Here dn/dM is the halo mass function for which we adopt a model of Tinker et al. (2008, 2010), $\tilde{u}_{\text{sat}}(k, M)$ is the Fourier

transform of the radial distribution of satellite galaxies normalised such that $\tilde{u}_{\text{sat}}(k, M) \rightarrow 1$ as $k \rightarrow 0$, $P_{\text{lin}}(k, z)$ is the linear matter power spectrum computed with CLASS (Blas et al. 2011), $\langle n_g(z) \rangle$ is the mean number density of galaxies given by

$$\langle n_g(z) \rangle = \int dM \frac{dn}{dM} (\langle N_{\text{cen}}|M \rangle + \langle N_{\text{sat}}|M \rangle), \quad (9)$$

and $b_g(k, z)$ is the scale-dependent galaxy bias given by

$$b_g(k, z) = \frac{1}{\langle n_g(z) \rangle} \int dM \frac{dn}{dM} [\langle N_{\text{cen}}|M \rangle + \langle N_{\text{sat}}|M \rangle \tilde{u}_{\text{sat}}(k, M)] b_1(M, z), \quad (10)$$

with a linear halo bias $b_1(M, z)$ of Tinker et al. (2010). The other functions, $\langle N_{\text{cen}}|M \rangle$ and $\langle N_{\text{sat}}|M \rangle$, are called the halo occupation distribution (HOD), and we shall describe them in Sec. 3.2.

We assume that the radial distribution of satellite galaxies in a halo follows an NFW profile (Navarro et al. 1997) characterized by a scale radius for galaxies $r_{s,g}$ up to some maximum radius $r_{\text{max},g}$:

$$u_{\text{sat}}(r) \propto \frac{1}{(r/r_{s,g})(r/r_{s,g} + 1)^2} \Theta(r_{\text{max},g} - r), \quad (11)$$

where Θ is the Heaviside step function. In figure 3, we show radial distribution profiles of member galaxies in the 16 largest galaxy clusters found in the low-density-contrast (LDC) catalog of 2MRS (Crook et al. 2007, 2008). We find that satellite galaxies are distributed out to 3–6 times r_{200} .³

The best-fitting values for the ratio of the scale radius of

³ The maximum radius $r_{\text{max},g}$ depends on how one defines galaxy clusters. In a more recent catalog of Tully (2015b), clusters are defined to be more compact than the LDC definition of Crook et al. (2007, 2008), yielding smaller values of $r_{\text{max},g}/r_{200}$. In order to accommodate this ambiguity, we shall treat $r_{\text{max},g}/r_{200}$ as a free parameter.

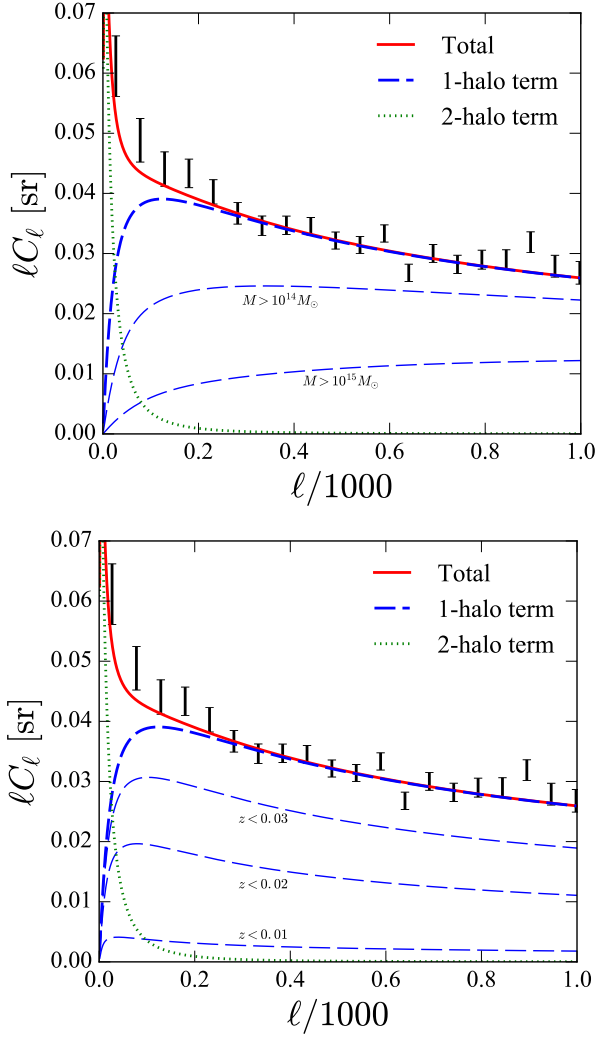


Figure 2. Angular power spectrum of the 2MRS galaxies, compared with the best-fitting model (solid; see Sec. 3). The one- and two-halo terms are shown as the thick dashed and the dotted curves, respectively. The thin dashed curves show contributions from mass ranges relevant for clusters of galaxies as indicated (top), and those from a few different redshift ranges (bottom). The error bars show the diagonal elements of the covariance matrix (see Sec. 2.3).

galaxies to that of dark matter $r_{g,s}/r_s$ vary across clusters. We use the mass-concentration relation of [Sánchez-Conde & Prada \(2014\)](#) to compute r_s as a function of halo masses, which are inferred from dynamical analysis of the member galaxies in each cluster ([Crook et al. 2007, 2008](#)). The solid curves in figure 3 show NFW profiles with the best-fitting $r_{s,g}/r_s$ from unbinned likelihood analysis. Since the parameter $r_{s,g}/r_s$ varies from cluster to cluster, and the cluster mass estimates as well as intrinsic scatter in mass-concentration relation are uncertain, we shall treat it as a free parameter.

The angular power spectrum is obtained by projecting $P_g(k, z)$ onto two-dimensional sky. Using Limber’s approximation, we obtain

$$C_\ell^g = \int \frac{d\chi}{\chi^2} W_g^2(z) P_g\left(\frac{\ell}{\chi}, z\right), \quad (12)$$

where χ is the comoving distance to a galaxy at a redshift z , and the function $W_g \equiv (d \ln N_g/dz)(d\chi/dz)^{-1}$ is computed with equation (2).

3.2 Halo Occupation Distribution

Following [Zheng et al. \(2005\)](#), we parameterize the HOD functions determining the mean number of central galaxies, $\langle N_{\text{cen}}|M \rangle$, and that of satellite galaxies, $\langle N_{\text{sat}}|M \rangle$, in a dark matter halo of mass M as

$$\langle N_{\text{cen}}|M \rangle = \frac{1}{2} \left[1 + \text{erf} \left(\frac{\log M - \log M_{\text{min}}}{\sigma_{\log M}} \right) \right], \quad (13)$$

$$\langle N_{\text{sat}}|M \rangle = \left(\frac{M - M_0}{M_1} \right)^\alpha \Theta(M - M_0), \quad (14)$$

where erf is the error function. We fix $\sigma_{\log M} = 0.15$ and $M_0 = M_{\text{min}}$. The latter assumption ensures that satellite galaxies form only in halos that host a central galaxy. We therefore have three HOD parameters $\{M_{\text{min}}, M_1, \alpha\}$.

We do not vary the HOD parameters as a function of z . In principle this approximation may break down for a magnitude-limited sample such as the 2MRS, as the dominant galaxy population may change depending on z . As the 2MRS is nearly volume-limited up to $z \approx 0.02$, it is safe to use the HOD up to that redshift; however, we need to be careful when interpreting the HOD parameters derived from the whole sample. We shall come back to this point later.

4 RESULTS AND INTERPRETATION

4.1 Posterior distribution of the model parameters

We use Bayes’ theorem to compute the posterior distribution of the model parameters $\boldsymbol{\vartheta}$ given the data \mathbf{d} , $P(\boldsymbol{\vartheta}|\mathbf{d})$, with $\boldsymbol{\vartheta} = (r_{\text{max},g}/r_{200}, r_{s,g}/r_s, \log M_{\text{min}}, \log M_1, \alpha)$ from the likelihood of the data given a model, $\mathcal{L}(\mathbf{d}|\boldsymbol{\vartheta})$:

$$P(\boldsymbol{\vartheta}|\mathbf{d}) \propto P(\boldsymbol{\vartheta}) \mathcal{L}(\mathbf{d}|\boldsymbol{\vartheta}). \quad (15)$$

We adopt flat priors on the model parameters, i.e., $P(\boldsymbol{\vartheta}) = \text{constant}$ within the parameter ranges given in the second row of Table 2 and $P(\boldsymbol{\vartheta}) = 0$ otherwise.

As for the data \mathbf{d} , we use the angular power spectrum of 2MRS galaxies $C_\ell^{2\text{MRS}}$, as well as the number of 2MRS galaxies up to $z = 0.01$, $N_{2\text{MRS}}^{z < 0.01} = 3200$, in which the sample is safely volume-limited. We approximate the likelihood of the data as a Gaussian:

$$\begin{aligned} -2 \ln \mathcal{L}(\mathbf{d}|\boldsymbol{\vartheta}) &= \sum_{\ell\ell'} \left[C_\ell^{\text{th}}(\boldsymbol{\vartheta}) - C_\ell^{2\text{MRS}} \right] \text{Cov}(C_\ell, C_{\ell'})^{-1} \\ &\quad \times \left[C_{\ell'}^{\text{th}}(\boldsymbol{\vartheta}) - C_{\ell'}^{2\text{MRS}} \right] \\ &\quad + \frac{[N_{\text{th}}^{z < 0.01}(\boldsymbol{\vartheta}) - N_{2\text{MRS}}^{z < 0.01}]^2}{N_{2\text{MRS}}^{z < 0.01}}. \end{aligned} \quad (16)$$

Here the quantities with ‘th’ represent the model predictions given $\boldsymbol{\vartheta}$, and $\text{Cov}(C_\ell, C_{\ell'})$ is the covariance matrix.

We use the Markov-Chain Monte Carlo (MCMC) to explore the parameter space. To this end we use the **MultiNest** ([Feroz & Hobson 2008; Feroz et al. 2009, 2013](#)) package for the MCMC and obtain the posterior distributions of the model parameters.

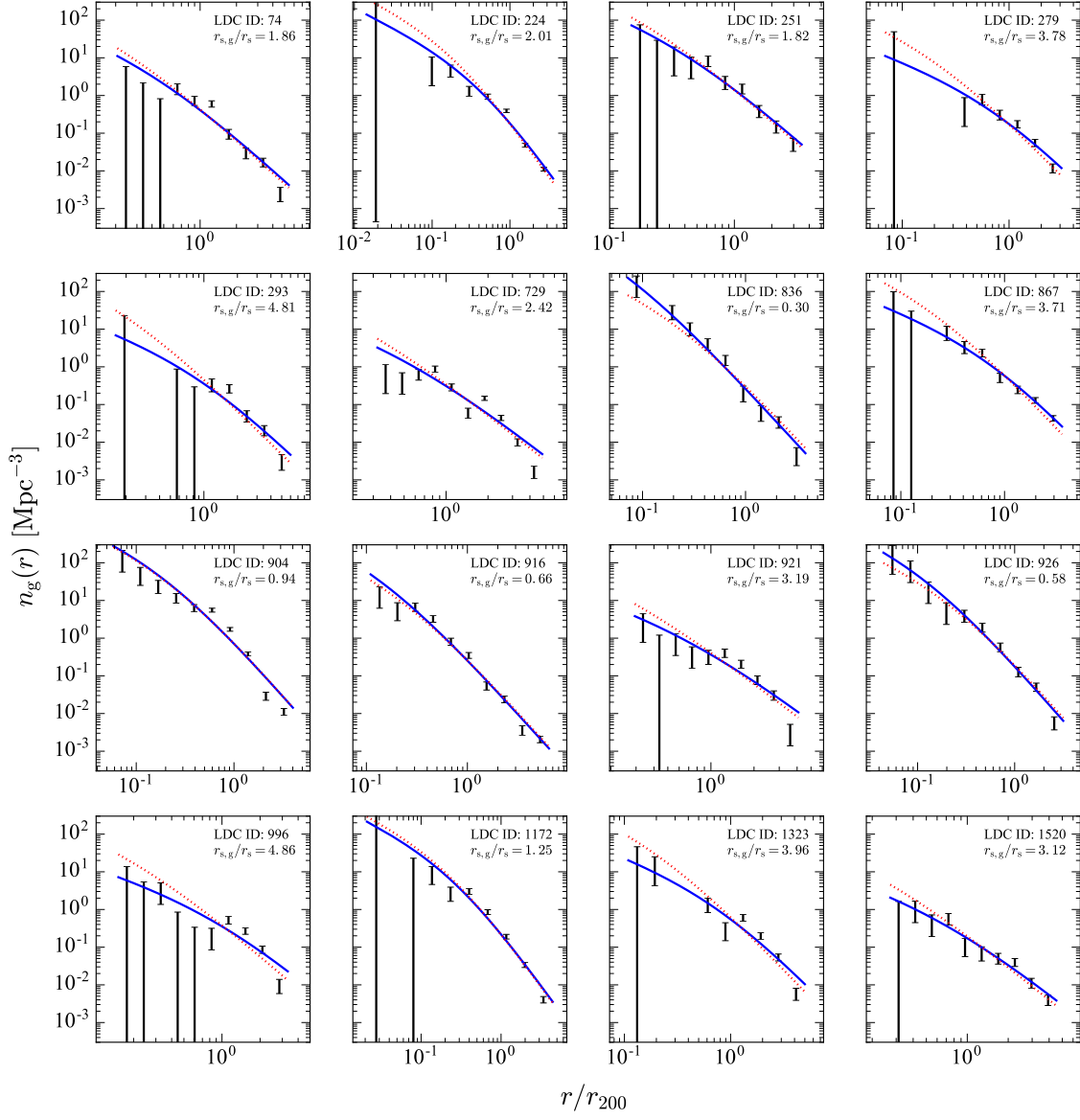


Figure 3. Number density profiles of member galaxies in the 16 largest galaxy clusters (with ID numbers) found in the LDC catalog of 2MRS galaxies (Crook et al. 2007, 2008). The solid and dotted curves show NFW profiles with the best-fitting $r_{s,g}/r_s$ and with a fixed $r_{s,g}/r_s = 1$, respectively.

Table 2. Medians and 1σ credible intervals of the posterior distributions of the model parameters, for three independent runs of computing the angular power spectrum. The second row shows the prior range, within which each parameter was drawn from a flat distribution. The last column shows χ^2_{\min} compared with a degree of freedom (dof).

Catalog	$r_{\max,g}/r_{200}$	$r_{s,g}/r_s$	$\log(M_{\min}/M_{\odot})$	$\log(M_1/M_{\odot})$	α	χ^2_{\min}/dof
Prior	0–15	0–15	9–14	9–14	0–2	
Run 1	$6.9^{+3.0}_{-1.7}$	$0.62^{+0.13}_{-0.12}$	$11.84^{+0.17}_{-0.14}$	$11.98^{+0.18}_{-0.24}$	$0.849^{+0.073}_{-0.088}$	33.3/16
Run 2	$6.4^{+3.1}_{-1.6}$	$0.72^{+0.15}_{-0.14}$	$11.87^{+0.19}_{-0.17}$	$11.97^{+0.21}_{-0.27}$	$0.855^{+0.087}_{-0.096}$	29.7/16
Run 3	$6.7^{+2.5}_{-1.5}$	$0.61^{+0.11}_{-0.10}$	$11.83^{+0.15}_{-0.13}$	$11.97^{+0.17}_{-0.21}$	$0.837^{+0.068}_{-0.074}$	47.2/16

As described in Sec. 2.3, we first run the MCMC with the Gaussian covariance matrix, and extract the best-fitting model parameters. We then use those parameters to calculate the trispectrum as

$$\begin{aligned}
T_{\ell\ell'} &= \int d\chi \frac{W_g^4(z)}{\chi^6 \langle n_g(z) \rangle^4} \int dM \frac{dn}{dM} \\
&\times \left[2 \langle N_{\text{sat}} | M \rangle \tilde{u}_{\text{sat}} \left(\frac{\ell}{\chi}, M \right) \right. \\
&\quad \left. + \langle N_{\text{sat}} | M \rangle^2 \left| \tilde{u}_{\text{sat}} \left(\frac{\ell}{\chi}, M \right) \right|^2 \right] \\
&\times \left[2 \langle N_{\text{sat}} | M \rangle \tilde{u}_{\text{sat}} \left(\frac{\ell'}{\chi}, M \right) \right. \\
&\quad \left. + \langle N_{\text{sat}} | M \rangle^2 \left| \tilde{u}_{\text{sat}} \left(\frac{\ell'}{\chi}, M \right) \right|^2 \right]. \quad (17)
\end{aligned}$$

We run the MCMC again to obtain the final results. We find good convergence of the MCMC chains.

Since we estimate the noise contribution to the power spectrum by randomly dividing the 2MRS catalog into two (see Sec. 2.2), the galaxy density field used for computing the power spectrum contains some randomness. To quantify the impacts of this randomness, we calculated three sets of density fields with different initial random seeds, and repeated the parameter estimation. The power spectrum shown in figure 2 is the first set “run 1”, whose posterior distribution of the parameters is shown in figure 4. The posterior distributions for the “run 2” and “run 3” are similar. The parameter values are summarized in Table 2. We find that all runs give similar results.

In the top panel of figure 2, we show the contributions from different ranges of halo masses. We find that the angular power spectrum is dominated by the one-halo term at $\ell \gtrsim 30$. In other words, the 2MRS angular power spectrum is dominated by galaxies residing in nearby galaxy clusters and groups.

The derived HOD parameters (Table 2) are reasonable: the galaxy distribution extends out to several times r_{200} ; the galaxy and dark matter scale radii are similar on average, with a slight preference for $r_{s,g}/r_s < 1$, though this parameter varies significantly across individual halos (see figure 3); the mass scales enter into the HOD are on the order of the Milky Way mass; and the number of satellite galaxies increases with the host halo mass slightly slower than a linear relation.

The best-fitting models give $\chi^2_{\text{min}} = -2 \ln \mathcal{L}_{\text{max}} = 33.3, 29.7$, and 47.2 for 16 degrees of freedom (i.e., 21 data points and 5 parameters) for the run 1 through 3. Taken at the face values, the probabilities to exceed (PTE) these χ^2_{min} are 6.7×10^{-3} , 2.0×10^{-2} , and 6.3×10^{-5} . These PTE are rather low except for the run 2. This may suggest that our HOD modeling is too simplistic, requiring more sophisticated ones instead. For example, as we stated in Sec. 3.2, the use of the HOD model for a magnitude-limited sample would introduce an error. (The 2MRS is nearly volume-limited up to $z \approx 0.02$.) Such modeling error would not only affect the model power spectrum, but also the covariance matrix via the trispectrum term, potentially changing a χ^2 value. Nonetheless, the model presented here will probably be good enough for interpreting various cross correlation results.

4.2 Contribution from the known galaxy groups and clusters

Figure 2 shows contributions from the mass ranges relevant for clusters of galaxies: $M > 10^{14} M_\odot$ and $> 10^{15} M_\odot$. We find that most of the power at small angular scales can be attributed to galaxies residing in galaxy clusters. We can test this result directly by summing up the contributions from galaxy groups and clusters we see in the 2MRS. We use recent group catalogs of 2MRS by Tully (2015b) and Lu et al. (2016).

We compute a contribution to the angular power spectrum from each of the groups and clusters as

$$C_\ell^c = \frac{4\pi}{N_{2\text{MRS}}^2} (N_g^c)^2 \left| \tilde{u}_g^c \left(\frac{\ell}{\chi_c}, M_c \right) \right|^2, \quad (18)$$

where “c” denotes a group or a cluster, and \tilde{u}_g^c is the Fourier transform of the NFW profile with the best-fitting $r_{s,g}$ and $r_{\text{max},g}$ for individual groups and clusters. Figure 5 shows contributions to C_ℓ from the catalogs with various numbers of member galaxies, $N_g \geq 50, \geq 20$, and ≥ 10 , in which there are 17, 78, and 299 groups and clusters, respectively.

We also show individual contributions from the 17 largest clusters. We find that about ten per cent of the power in sub-degree angular scales comes from these 17 clusters that host more than 50 member galaxies. The remaining power comes from hundreds of galaxy groups and clusters. For smaller groups, the approximation used in equation (18) becomes less valid, because one can no longer regard the galaxy distribution as given by the smooth NFW function. Nonetheless figure 5 provides a useful cross-check of our result.

In the top panel of figure 6, we show the numbers of member galaxies found in each group or cluster in the Tully (2015b) catalog as a function of its virial mass M_{vir} . We estimate the virial mass of the groups and clusters through equation (4) of Tully (2015a) and a proper conversion from M_{200} to M_{vir} afterwards. We also show the 68% and 95% credible intervals for the mean galaxy number, $\langle N_g | M \rangle \equiv \langle N_{\text{cen}} | M \rangle + \langle N_{\text{sat}} | M \rangle$, from the posterior distribution of the HOD parameters of the “run 1”. The bottom panel of figure 6 shows the same, but for an independent 2MRS group catalog by Lu et al. (2016).

The HOD parameters are intrinsic to the galaxies. To compare with the observation, we correct for the selection effect as follows. The number density of the *observed* galaxies is estimated from the redshift distribution [equation (2)] as $n_{2\text{MRS}}(z) = (dN_g/dz)(d\chi/dz)^{-1}/(4\pi f_{\text{sky}}\chi^2)$, while the *intrinsic* density is given by $n_{\text{HOD}}(z) = \langle n_g(z) \rangle$ from equation (9). In figure 6, for each of the three subsamples (with mean redshifts of $\bar{z} = 0.0065, 0.016$, and 0.025 for Tully (2015b) and $\bar{z} = 0.0067, 0.016$, and 0.025 for Lu et al. (2016)), we re-scale the total number of member galaxies $\langle N_g | M \rangle$ by $n_{2\text{MRS}}(\bar{z})/n_{\text{HOD}}(\bar{z})$. We see very good agreement between the HOD model and the observation of the groups and clusters, justifying our model.

5 CONCLUSION

We have presented the measurement and interpretation of the angular power spectrum of the 2MRS. We found that the 2MRS galaxies are so highly clustered that the power

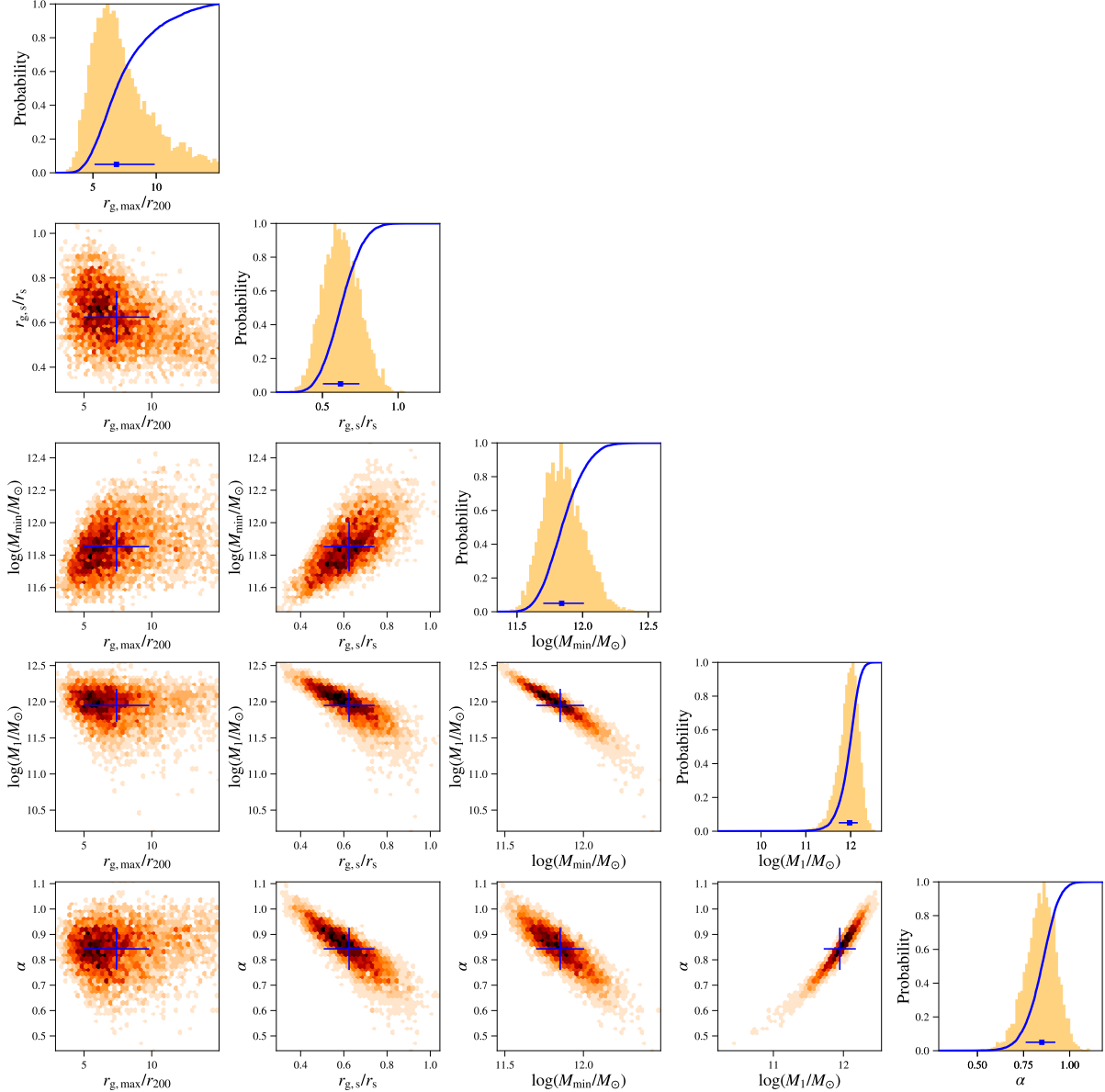


Figure 4. Posterior distribution of the model parameters. The diagonal panels show the one-dimensional distribution marginalised over the other parameters as well as the cumulative distribution (line). The other panels show the two-dimensional marginalised joint distributions. The cross symbols show the mean and the 1σ uncertainty.

spectrum at $\ell \gtrsim 30$ is dominated by the one-halo term, i.e., galaxies residing in nearby galaxy groups and clusters. We demonstrated this by the HOD modeling of the power spectrum, as well as by directly summing up the contributions from groups and clusters identified in the 2MRS catalog.

This property makes the 2MRS catalog well suited for cross-correlation studies with other tracers of groups and clusters, e.g., hot gas traced by the thermal Sunyaev-Zeldovich effect (Makiya et al. 2017), gamma-rays from annihilation of dark matter particles in sub-halos of groups and clusters (Ando et al. 2014), and so on. Properly interpreting such cross-correlation measurements requires accurate information of clustering statistics of the 2MRS galaxies, and our measurement and HOD model provide the required information.

ACKNOWLEDGMENTS

We thank Lucas Macri for providing us with the 2MRS catalog. This work was supported by the Netherlands Organization for Scientific Research (NWO) through Vidi grant (SA), and also in part by JSPS KAKENHI Grants, JP15H05896 (EK) and JP17H04836 (SA). We acknowledge the use of HEALPix (Górski et al. 2005) and PolSpice (Szapudi et al. 2001) packages.

REFERENCES

Afshordi, N., Loh, Y.-S., & Strauss, M. A. 2004, Phys. Rev. D, 69, 083524

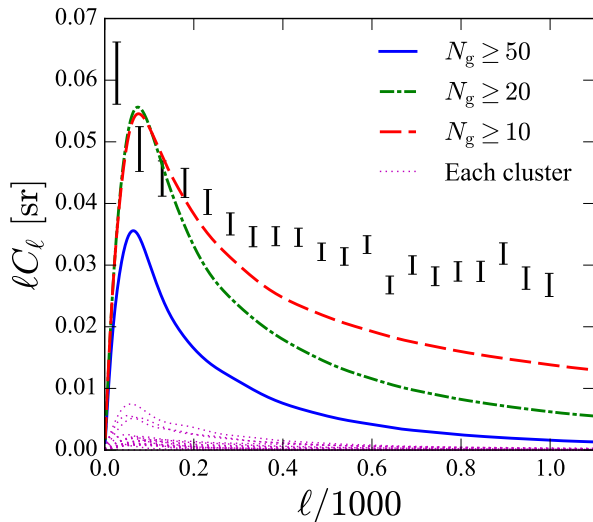


Figure 5. Angular power spectrum of galaxies residing in groups and clusters detected in the 2MRS. The cumulative contributions from groups and clusters above a certain size are shown as the solid ($N_g \geq 50$), dot-dashed ($N_g \geq 20$), and dashed ($N_g \geq 10$) curves. There are 17, 78, and 299 groups and clusters containing 1578, 3376, and 6217 galaxies in these samples respectively. The dotted curves show C_ℓ from each of the 17 largest clusters.

Ando, S., Benoit-Lévy, A., & Komatsu, E. 2014, *Phys. Rev. D*, 90, 023514
 Baldauf, T., Seljak, U., Smith, R. E., Hamaus, N., & Desjacques, V. 2013, *Phys. Rev. D*, 88, 083507
 Blas, D., Lesgourgues, J., & Tram, T. 2011, *J. Cosmology Astropart. Phys.*, 7, 034
 Bryan, G. L., & Norman, M. L. 1998, *ApJ*, 495, 80
 Crook, A. C., Huchra, J. P., Martimbeau, N., et al. 2007, *ApJ*, 655, 790
 Crook, A. C., Huchra, J. P., Martimbeau, N., et al. 2008, *ApJ*, 685, 1320
 Cuoco, A., et al. 2015, *ApJS*, 221, 29
 Feroz, F., & Hobson, M. P. 2008, *MNRAS*, 384, 449
 Feroz, F., Hobson, M. P., & Bridges, M. 2009, *MNRAS*, 398, 1601
 Feroz, F., Hobson, M. P., Cameron, E., & Pettitt, A. N. 2013, *arXiv:1306.2144*
 Frith, W. J., Outram, P. J., & Shanks, T. 2005, *MNRAS*, 364, 593
 Górski K.M. et al. 2005, *ApJ*, 622, 759
 Hu, W., & Kravtsov, A. V. 2003, *ApJ*, 584, 702
 Huchra, J. P., et al. 2012, *ApJS*, 199, 26
 Komatsu, E., & Seljak, U. 2002, *MNRAS*, 336, 1256
 Lavaux, G. and Hudson, M. J. 2011, *MNRAS*, 416, 2840
 Lu, Y., Yang, X., Shi, F., et al. 2016, *ApJ*, 832, 39
 Makiya, R., Komatsu, E., Ando, S., & Benoit-Lévy, A. 2017, in preparation
 Navarro, J. F., Frenk, C. S., & White, S. D. M. 1997, *ApJ*, 490, 493
 Planck Collaboration 2016a, *A&A*, 594, A22
 Planck Collaboration 2016b, *A&A*, 594, A13
 Sánchez-Conde, M. A., & Prada, F. 2014, *MNRAS*, 442, 2271
 Seljak, U. 2000, *MNRAS*, 318, 203
 Skrutskie, M. F., et al. 2006, *AJ*, 131, 1163
 Szapudi, I., Prunet, S., Colombi, S. 2001, *ApJ*, 561, L11
 Tinker, J. L., et al. 2008, *ApJ*, 688, 709
 Tinker, J. L., et al. 2010, *ApJ*, 724, 878
 Tully, R. B. 2015a, *AJ*, 149, 54

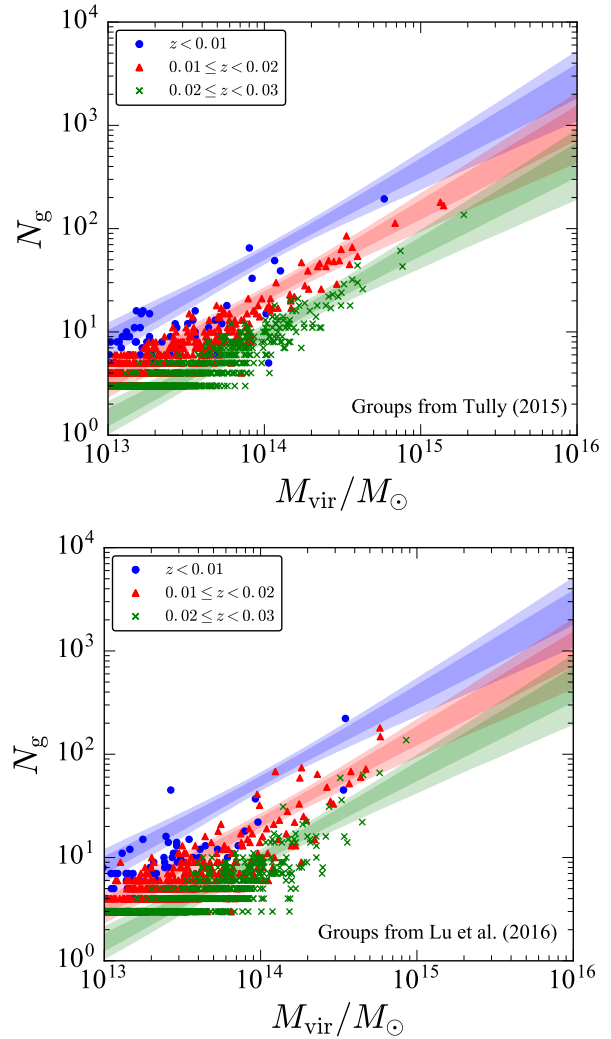


Figure 6. Numbers of member galaxies in groups and clusters of galaxies in the Tully (2015b, top) and Lu et al. (2016, bottom) catalogs. Different symbols show different redshift ranges. The thick and thin bands are the 68% and 95% credible intervals for the mean galaxy number predicted by the HOD model, $\langle N_g | M \rangle$, after the selection effect has been corrected for each of these three subsamples (see text).

Tully, R. B. 2015b, *AJ*, 149, 171
 Xia, J.-Q., Cuoco A., Branchini, E., Fornasa, M., & Viel M. 2011, *MNRAS*, 416, 2247
 Zheng, Z., et al. 2005, *ApJ*, 633, 791